

RESEARCH

Open Access



Interleukin-2 improves insulin sensitivity through hypothalamic sympathetic activation in obese mice

Subin Moon^{1†}, Yejin Park^{1†}, Sooyeon Jang¹, Saeha Kim¹, Dan-Gyeong Song¹, Dae-Chul Shin¹ and Chan Hee Lee^{1,2*}

Abstract

Background IL-2 regulates T cell differentiation: low-dose IL-2 induces immunoregulatory Treg differentiation, while high-dose IL-2 acts as a potent activator of cytotoxic T cells and NK cells. Therefore, high-dose IL-2 has been studied for use in cancer immunotherapy. We aimed to utilize low-dose IL-2 to treat inflammatory diseases such as obesity and insulin resistance, which involve low-grade chronic inflammation.

Main body Systemic administration of low-dose IL-2 increased Treg cells and decreased inflammation in gonadal white adipose tissue (gWAT), leading to improved insulin sensitivity in high-fat diet-fed obese mice. Additionally, central administration of IL-2 significantly enhanced insulin sensitivity through the activation of the sympathetic nervous system. The sympathetic signaling induced by central IL-2 administration not only decreased interferon γ (IFN γ) + Th1 cells and the expression of pro-inflammatory cytokines, including *Il-1 β* , *Il-6*, and *Il-8*, but also increased CD4 + CD25 + FoxP3 + Treg cells and *Tgfb* expression in the gWAT of obese mice. These phenomena were accompanied by hypothalamic microgliosis and activation of pro-opiomelanocortin neurons. Furthermore, sympathetic denervation in gWAT reversed the enhanced insulin sensitivity and immune cell polarization induced by central IL-2 administration.

Conclusion Overall, we demonstrated that IL-2 improves insulin sensitivity through two mechanisms: direct action on CD4 + T cells and via the neuro-immune axis triggered by hypothalamic microgliosis.

Keywords Interleukin-2, Insulin resistance, Adipose tissue inflammation, Sympathetic nervous system, Hypothalamic microglia, Pro-opiomelanocortin (POMC) neurons

[†]Subin Moon and Yejin Park contributed equally to this work.

*Correspondence:

Chan Hee Lee
chl22@hallym.ac.kr

¹Department of Biomedical Science, Hallym University,
Chuncheon 24252, Republic of Korea

²Program of Material Science for Medicine and Pharmaceutics, Hallym
University, Chuncheon 24252, Republic of Korea



© The Author(s) 2024. **Open Access** This article is licensed under a Creative Commons Attribution-NonCommercial-NoDerivatives 4.0 International License, which permits any non-commercial use, sharing, distribution and reproduction in any medium or format, as long as you give appropriate credit to the original author(s) and the source, provide a link to the Creative Commons licence, and indicate if you modified the licensed material. You do not have permission under this licence to share adapted material derived from this article or parts of it. The images or other third party material in this article are included in the article's Creative Commons licence, unless indicated otherwise in a credit line to the material. If material is not included in the article's Creative Commons licence and your intended use is not permitted by statutory regulation or exceeds the permitted use, you will need to obtain permission directly from the copyright holder. To view a copy of this licence, visit <http://creativecommons.org/licenses/by-nc-nd/4.0/>.

Introduction

IL-2 was first introduced as a ‘T-cell growth factor’ in 1976 [1], and its use has since been applied in cancer immunotherapy [2]. Several clinical studies demonstrated that IL-2 therapy displayed tumor-preventing characteristics, where IL-2 administration results in prominent regression of metastatic cancers [3, 4]. Based on these results, IL-2 was granted US Food and Drug Administration approval for metastatic cancer treatment in 1992 [5]. However, owing to the potential toxicity of IL-2 in inducing vascular leak syndrome (VLS), its immunotherapeutic application has been limited to eligible patients with cancer [6, 7]. Another challenge in using IL-2 in cancer therapy is that IL-2 stimulates both cytotoxic cells, such as natural killer (NK) cells and effector T cells, as well as immunosuppressive cells, such as regulatory T (Treg) cells, indicating its dual functional properties [8].

The ‘dual functional property’ of IL-2 on the immune response depends on the combination of IL-2 receptor (IL-2R) chains [9, 10]. IL-2R is composed of three chains, including IL-2R α (CD25), IL-2R β (CD122), and IL-2R γ (CD132). Each chain constitutes a part of IL-2R and directly binds to IL-2 with different affinities depending on the combination of chains (α , $\beta\gamma$, and $\alpha\beta\gamma$). For instance, low- and high-dose IL-2 lead to immunosuppression, preferentially activating IL-2R $\alpha\beta\gamma$ expressed in Treg cells (CD4+CD25+Foxp3+) with high affinity. However, high-dose IL-2 triggers a cytotoxic reaction that activates IL-2R $\beta\gamma$ expressed in NK cells, memory T cells, and effector T cells with low or intermediate affinities [9]. The limitation of IL-2 therapy, resulting in unwanted outcomes, is associated with these differential interactions between IL-2 and IL-2R subunits.

Some studies have used low-dose IL-2 to ameliorate inflammation due to its immunoregulatory properties [11–13]. Short-term (5 days or 10 days) administration of low-dose IL-2 promoted Treg cell survival and suppressed interferon γ (IFN γ) production in pancreatic T cells in nonobese diabetic (NOD) mice [12]. Clinical data showed that combination therapy of low-dose IL-2 with exogenous Treg cells for 5 consecutive days resulted in enhanced Treg survival and expansion [14]. However, no evidence has been reported regarding whether or how low-dose IL-2 attenuates obesity-associated metabolic disorders such as glucose intolerance or insulin resistance.

The hypothalamus plays a central role in regulating food intake and energy metabolism [15]. Hypothalamic neurons, such as pro-opiomelanocortin (POMC) and agouti-related protein (AgRP) neurons, complementarily regulate metabolic homeostasis in the body [15]. The activity of these neurons can be altered by the activation of neighboring glial cells such as astrocytes, microglia, or bone marrow-derived macrophages [16, 17]. Chronic

microglial activation induces metabolic complications, such as hyperphagia-induced obesity, glucose intolerance, and insulin resistance, by interfering with the activity of POMC neurons [16, 18, 19]. However, other studies have shown that microglial activation activates POMC neurons, leading to anorexia and weight loss by suppressing the inhibitory synapse of POMC neurons [20, 21]. These conflicting results suggest that further studies are required to explore the role of hypothalamic microglial activation in the development of obesity and metabolic disorders.

In this study, we examined the metabolic effects of IL-2 in high-fat diet (HFD)-fed obese mice (DIO mice) and changes in immune cell polarization in gonadal white adipose tissue (gWAT). Moreover, we investigated whether this mechanism could be initiated by hypothalamic neurons or glial cells, emphasizing a neuro-immune axis centered around the hypothalamus.

Materials and methods

Mice

Seven-week-old C57BL/6J male mice were purchased from DBL (Chungbuk, South Korea). Seven-week-old mice underwent at least a one-week acclimation period and were then independently housed in a temperature-controlled room (22 \pm 1 °C) with a 12 h light-dark cycle (lights on 8 a.m.). Mice were given free access to water and either a chow diet (CD) (Cargil Agri Purina, #EEGJ30060) or a 60% HFD (Research Diet, #D12492). Body weight and food intake were measured daily between 9:00 and 10:00 a.m. throughout the experimental period. All experimental procedures were approved by the Institutional Animal Care and Use Committee (IACUC) of Hallym University (Hallym R1 #2022-72).

Drug administration and experimental design

To investigate the effects of IL-2 on body weight, food intake, and systemic metabolism in HFD-fed mice, recombinant IL-2 (PeproTech, #200-02) was administered intraperitoneally (IP) at the concentrations indicated in each figure. To examine the systemic effects of IL-2, HFD-fed mice for 2 weeks were treated with IL-2 IP for 12 days. The study included three groups: vehicle ($n=5$), low-dose IL-2 ($n=5$), and high-dose IL-2 ($n=5$). Low-dose IL-2 was administered at 1,000 IU/day, while high-dose IL-2 was administered at 100,000 IU/day, as indicated by previous studies [22]. Body weight and food intake were measured daily throughout the study period. The glucose tolerance test (GTT) and insulin tolerance test (ITT) were conducted twice, on the 5th and 9th days after the first administration. Twelve days after injection, the mice were sacrificed, and cardiac perfusion for histological and flow cytometry (FACS) analyses was performed. To examine the metabolic effects of lower IL-2

doses, including 10 IU and 100 IU, mice were divided into three groups: vehicle ($n=4$), 10 IU IL-2 ($n=5$), and 100 IU IL-2 ($n=5$). Body weight, food intake, ITT, and FACS analysis were performed at the same time points as described above. To investigate the central effects of IL-2, the mice were divided into three groups: vehicle ($n=4$), 1 IU IL-2 ($n=4$ for FACS analysis, $n=5$ for metabolic analysis), and 10 IU IL-2 ($n=5$). Mice underwent stereotaxic cannulation followed by intracerebroventricular (ICV) administration of IL-2 at doses of 1 and 10 IU/day. Body weight and food intake were measured for 10 days, and GTT and ITT were performed on the 4th and 8th days. Mice were sacrificed on the 10th day post-administration for histological and FACS analysis. For the pair-feeding study, six mice were centrally administered IL-2, while five pair-fed mice received the same amount of food consumed by the IL-2 group over the previous 24 h, and were administered vehicle. Body weight, food intake, ITT, histological analysis of brown adipose tissue (BAT) and inguinal white adipose tissue (iWAT), and FACS analysis were conducted on the indicated days. To confirm whether IL-2 administered via IP crosses the blood-brain barrier and enters the hypothalamus, biotinylated IL-2 (Acro Biosystems, #IP2-H82E4) was administered intraperitoneally. The experimental procedures followed a previous report [23]. Three hours after biotinylated IL-2 administration, the mouse brains were collected, sectioned, and stained with PE-conjugated Streptavidin (Acro Biosystems, #STN-NP119). To investigate the role of the sympathetic nervous system (SNS), six mice were assigned to the control group, and seven mice were assigned to the sympathetic denervation group. Sympathetic denervation was performed using 6-hydroxydopamine (6-OHDA) (10 mg/mL, Sigma, #4381) dissolved in 1% ascorbic acid (AA) (Sigma, #A4403). 1% AA or 6-OHDA was injected into the gWAT fat pad using a Hamilton syringe (Hamilton Company, #87930) on the same day as cannulation.

Metabolic phenotyping

For the Oral Glucose Tolerance Test (OGTT), glucose (1 g/kg, Sigma, #G8270) was orally administered following an overnight fast. For the Intraperitoneal Insulin Tolerance Test (IPITT), insulin (Humulin-R® 0.25 U/kg, Eli Lilly, #170131BIJ) was injected intraperitoneally into the mice following an overnight fast. Blood samples were collected from the tail vein at indicated timepoints after glucose or insulin injection, and glucose levels were measured using a glucometer (ACCU-CHEK®, Aviva Plus System). To assess insulin sensitivity in peripheral tissues, mice were injected with insulin (0.25 U/kg) into the peritoneal cavity, and tissues were quickly obtained 10 min later. Insulin sensitivity was analyzed by calculating

the ratio of phosphorylated AKT (pAKT) to total AKT (tAKT) protein levels.

Flow cytometry analysis

gWATs were collected from mice, then dissected and converted into single cells by chopping and digestion using an Adipose Tissue Dissociation Kit (Milteny Biotec, #130-105-808) and a gentleMACS Octo Dissociator with Heaters (Milteny Biotec, #130-096-427). The stromal vascular cell (SVC) fractions were obtained by separating them from red blood cells (RBCs) using ACK (Ammonium-Chloride-Potassium) lysis buffer (NH_4Cl , KHCO_3 , and EDTA). For transcription factor staining, SVCs were incubated in Iscove's modified Dulbecco's medium (IMDM) (10%FBS, 1%P/S) treated with PMA (Sigma-Aldrich, #P8139), ionomycin (Sigma-Aldrich, #I0634), and Golgi stop (BD Bioscience, #554724) for 6 h, followed by staining with the relevant antibodies. The SVCs were incubated for 30 min in FACS wash buffer (1%FBS, 2mM EDTA, and 0.05% NaN_3) containing an Fc blocker (BD Bioscience, #553142) and 7-AAD (1:62.5, Invitrogen, #A1310). After washing with FACS wash buffer, the SVCs were incubated with a transcription factor staining buffer kit (Invitrogen, #00-5523-00) for 30 min to analyze the CD4+T cells. The SVCs were treated for 30 min in 'Antibody cocktail 1' against CD4 (1:250, BD Pharmingen, #553046), FoxP3 (1:62.5, Invitrogen, #12-4771-82), IFN γ (1:250, BD Pharmingen, #554413), T cell receptor β (TCR β) (1:125, Invitrogen, #47-5961-82), CD25 (1:500, BD Horizon, #562606), and CD45 (1:250, BioLegend, #103151). To analyze adipose tissue macrophages (ATMs), SVCs were fixed in paraformaldehyde (PFA) (Tech&Innovation, #BPP-9004) for 10 min. After washing with FACS wash buffer, SVCs were permeabilized with saponin buffer (Sigma-Aldrich, #47036, 0.2% in FACS wash buffer) for 10 min at room temperature (RT). The SVCs were treated for 30 min in 'Antibody cocktail 2' against CD11b (1:250, BD Pharmingen, #557396), CD11c (1:250, Invitrogen, #12-0114-81), Ly6G (1:167, BD Pharmingen, #560601), CD206 (1:250, BD Pharmingen, #565250), I-A/I-E (1:500, eBioscience, #47-5321-82), F4/80 (1:100, BD Horizon, #563900), and CD45 (1:250, BioLegend, #103151). To analyze T and B cells, the SVCs were incubated for 30 min in 'Antibody cocktail 3' against CD11b (1:250, BD Pharmingen, #557396), Ly-6 C (1:832.5, eBioscience, #12-5932-80), 7-AAD (1:62.5, Invitrogen, #A1310), Ly-6G (1:167.5, BD Biosciences, #560601), CD5 (1:500, eScience, #17-0051-81), B220 (1:250, eScience, #47-0452-80), CD45 (1:250, BioLegend, #103151) and Fc-blocker (1:50, BD Bioscience, #553142). To analyze CD4+ and CD8+T cells, the SVCs were incubated for 30 min in 'Antibody cocktail 4' against CD44 (1:250, BD Biosciences, #561859), 7-AAD (1:62.5, Invitrogen, #A1310), CD62L (1:2500, BD Biosciences,

#560516), CD4 (1:250, BD Biosciences, #553051), TCR β (1:125, eScience, #47-5961-82), CD45 (1:250, BioLegend, #103151), and Fc-blocker (1:50, BD Bioscience, #553142). All samples were measured using the FACS-CantoII instrument (BD Biosciences) and analyzed using FlowJo software (Ver. 10.8).

Quantitative PCR analysis

To measure mRNA expression, total RNA was extracted from tissue samples using the TRIzol reagent (Thermo Fisher, #15596018). Subsequently, cDNA synthesis was performed, and quantitative PCR was conducted using the SYBR green premix (BIONEER, #K-6253) and primers (*Scad*, *Perilipin*, *Atgl*, *Hsl*, *Il-2 α* , *Il-2 β* , *Il-2 γ* , *Il-1 β* , *Il-6*, *Il-8*, *Tnf α* , *Il-4*, *Il-10*, *Tgfb*, *Adrb2*, and *Adrb3*) detailed in Table S1. The quantitative analysis was conducted using the $\Delta\Delta$ CT method, with mRNA expression levels normalized to glyceraldehyde 3-phosphate dehydrogenase (*Gapdh*).

Cannulation and intracerebroventricular injection

Stereotaxic surgery was performed on C57BL/6J male mice aged over 8 weeks under anesthesia with isoflurane (Hana Pharm Co., Ltd.). To induce anesthesia, the mice were placed in a chamber with 2% isoflurane for 2–3 min. During the stereotaxic surgery, isoflurane was continuously administered at a concentration of 1.5% or less through the respiratory system. 26-gauge stainless steel guide cannulas (P1 Technologies, #C313G/SPC) were implanted into the lateral ventricle of the mice at stereotaxic coordinates of 0.6 mm caudal to bregma, 1 mm right to the sagittal sinus, and 2.0 mm ventral to the sagittal sinus. The guide cannula was fixed to the skull using dental cement (Vertex Resin Self-Curing; Dentimax BV., Netherlands). Throughout the procedure, a dummy cannula (P1 Technologies, #C313DC/SPC) was inserted into the guide cannula, except during drug injections, which were administered via the internal cannula (P1 Technologies, #C313I/SPC). To verify proper cannula placement, each mouse received 50 ng of angiotensin-2 (Sigma, #A9525) after a recovery period of 7 days. All solutions or drugs used in this study were delivered at a rate of 5 μ g/min using a Harvard apparatus (#70-2000) with a dose volume of 2 μ L.

Western blotting

Adipose tissues were lysed in radio-immunoprecipitation assay buffer (Biosesang, #RC2002-050-00) containing protease inhibitors (GenDEPOT, #P3100) and phosphatase inhibitors (GenDEPOT, #P3200). The lysates were centrifuged at 13,000 rpm for 30 min at 4 °C. Protein samples were separated on a 12% SDS-PAGE gel and transferred onto a PVDF membrane (Millipore, #IPVH00010). The membranes were blocked for 1 h in 3% skim milk

(Carl Roth, #T145.1) in 1X TBST buffer (Tween 20, Tris, and NaCl). Subsequently, membranes were incubated overnight at 4 °C with primary antibodies against pAKT (1:1000, Cell signaling, #9271), AKT (1:1000, Cell signaling, #9272), Uncoupling Protein-1 (UCP-1) (1:1000, Santa Cruz, #sc-293418), Tyrosine Hydroxylase (TH) (1:1000, Abcam, #AB137869) and α -tubulin (1:3000, Cell signaling, #3873). After washing with 1X TBST buffer, the membranes were incubated with anti-rabbit IgG, horseradish peroxidase (HRP)-linked antibody (1:1000, Cell Signaling, #7074), and anti-mouse IgG, HRP-linked antibody (1:1000, Cell Signaling, #7076) at RT for 1 h. Proteins were visualized using a chemiluminescence imaging system (GE Healthcare, ImageQuant LAS 500). Quantification of the protein bands was conducted using ImageJ (Ver. 1.8.0).

ELISA

To measure circulating corticosterone levels, blood samples were collected and incubated at RT for 2 h following the manufacturer's instructions. The samples were then centrifuged at 4 °C, 2,000 g for 20 min. Serum corticosterone levels were determined using a corticosterone ELISA kit (Abcam, #ab108821). To measure norepinephrine (NE) levels, gWAT tissues were collected from mice at 0 and 30 min after central IL-2 administration. NE levels in gWAT were measured using an NE ELISA Kit (Abcam, #ab287789). To examine cAMP levels in gWAT, tissue samples were collected at 0 and 30 min post-IL-2 administration, and cAMP levels were determined using a cAMP ELISA kit (ENZO, #ADI-900-067). All procedures were conducted according to the manufacturers' protocols, and optical densities were measured using a NanoQuant (TECAN, Infinite M200 Pro).

Immunostaining

For cardiac perfusion, all the mice were anesthetized with isoflurane. For tissue fixation, the mice were transcardially perfused with 50 mL of pre-cooled saline and 50 mL of pre-cooled 4% paraformaldehyde (PFA). The mouse brains were collected and post-fixed with 4% PFA for 16 h at 4 °C. For dehydration, the brains were placed in a 30% sucrose solution for 48 h at 4 °C. After the brain sink, the hypothalamic slices were obtained by sectioning coronally every 40 μ m using a cryostat (Leica, Wetzlar, Germany). For hypothalamic microglia staining, the brain slices were permeabilized with PBS containing 0.5% Triton X-100 (0.5% PBST) at RT for 5 min. Then, they were blocked with 3% donkey serum in 0.1% PBST at RT for 1 h. The hypothalamic slices were incubated with anti-mouse Iba1 antibody (1:400, Abcam, #ab5076) in a blocking solution at 4 °C for 16 h. After washing with 1X PBS, the sections were incubated with an appropriate Alexa-Fluor secondary antibody diluted 1:1000 at RT

for 1 h. For POMC-cFos double staining, the brain slices were blocked with 3% bovine serum albumin (BSA) in 0.5% PBST at RT for 1 h. The slices were incubated with antibodies against anti-mouse cFos (1:1000, Synaptic Systems, #226003) at 4 °C for 16 h. After washing with 1X PBS, the slices were incubated with the Alexa-Fluor 555 secondary antibody (1:1000, Invitrogen, #A31572) at RT for 1 h. The slides were then permeabilized with 0.5% PBST at RT for 5 min. Then they were blocked again with 3% BSA in a 0.5% PBST solution at RT for 1 h. After which, they were incubated with an antibody against anti-mouse β -endorphin antibody (1:1000, Phoenix Pharmaceuticals, #H-022-33) in the blocking solution at 4 °C for 16 h. Subsequently, the sections were incubated with the Alexa-Fluor 488 secondary antibody (1:1000, Invitrogen, #A21206). For microglia-POMC double staining, slides that had undergone Iba1 staining were then blocked with 3% BSA in 0.5% PBST solution and incubated with β -endorphin antibody in the blocking solution at 4 °C for 16 h. After washing with 1X PBS, the slides were incubated with the appropriate Alexa-Fluor secondary antibody. For microglia-IL-2R double staining, slides were permeabilized in 0.5% PBST for 5 min, then blocked with 5% horse serum in 0.5% PBST at RT for 1 h. Slides were incubated at 4 °C for 16 h with blocking solution containing anti-mouse IL-2R α (1:200, Santa Cruz, #sc-393326; Epitope: amino acids 23–49 at the N-terminus) or anti-mouse IL-2R β (1:200, Santa Cruz, #sc-166427; Epitope: amino acids 502–533 near the C-terminus) or anti-mouse IL-2R γ (1:200, Santa Cruz, #sc-271060; Epitope: amino acids 342–369 near the C-terminus) antibodies, respectively. Then the slides were conducted with the appropriate Alexa-Fluor secondary antibody at RT for 1 h. The subsequent Iba1 staining was performed as described above. For biotinylated IL-2 staining, brain slices from mice injected with biotinylated IL-2 were incubated with PE-conjugated Streptavidin (1:1,000) for 2 h at RT. Immunofluorescence images were captured using a confocal microscope (Carl Zeiss, #710) and a fluorescence microscope (Carl Zeiss, #430035-9061-00).

Hematoxylin & Eosin staining

To analyze the adipocyte sizes in BAT, iWAT, and gWAT, were harvested and fixed in pre-cooled 4% PFA. The adipose tissues were processed in ethanol and xylene using an automatic benchtop tissue processor (Leica, TP1020) and embedded in paraffin using a paraffin embedding station (Leica, EG1150). The samples were sectioned using a Rotary Microtome (Leica, RM2255). To stain the nuclei and cytoplasm of adipocytes, the slices were immersed in xylene (Reagents DUKSAN, #UN1307) for 15 min, followed by a series of ethanol solutions (100%, 95%, 90%, 80%, and 70%) for 5 min each. The slices were then stained with hematoxylin (Cancer Diagnostics, Inc.,

#SH3777) and eosin (BBC Biochemical, #3610) for 5 min each. The sections were dehydrated through a graded series of ethanol solutions (70%, 80%, 90%, 95%, and 100%) for 5 min each. Finally, the sections were exposed to xylene for 10 min. Images were captured using a microscope (Nikon, ECLIPSE Ni-U), and the adipocyte sizes were analyzed using Fiji software (Ver. 2.15.1).

Statistical analysis

The data are presented as the mean \pm standard error of the mean (SEM). Statistical analyses were performed using Prism software (GraphPad, Ver. 10.2.2). Group differences were evaluated using one-way, two-way, or repeated-measures ANOVA, followed by post-hoc least significant difference tests or unpaired two-sided Student's t-tests. Statistical significance was set at $p < 0.05$.

Results

Systemic administration of low-dose IL-2 improved insulin sensitivity in obese mice

An HFD induces systemic low-grade inflammation, leading to metabolic disorders such as glucose intolerance and insulin resistance [24]. Given that low-dose IL-2 has anti-inflammatory effects by regulating T cell differentiation [9], we hypothesized that low-dose IL-2 administration could ameliorate HFD-induced inflammatory metabolic disorders. To verify this hypothesis, intraperitoneal low-dose IL-2 (1,000 IU/day) or high-dose IL-2 (100,000 IU/day) was administered to HFD-fed C57BL/6J male mice (Fig. 1A). The IL-2 doses were based on previous studies [25]. Either low-dose IL-2 or high-dose IL-2 was administered for 12 days, during which no differences were observed in body weight, food intake, or glucose tolerance compared to the control group (Fig. 1B–D). However, insulin sensitivity was significantly improved by low-dose IL-2 administration, but not by high-dose IL-2 administration compared to the control group (Fig. 1E). To determine the minimal dose of IL-2 needed to enhance insulin sensitivity, lower doses of IL-2 (10 IU/day and 100 IU/day) were administered (Fig. S1A). Compared to the vehicle group, neither dose significantly affected body weight, food intake, or insulin sensitivity (Fig. S1B–D). These results suggest that at least 1,000 IU/day of IL-2 is required to improve insulin sensitivity in DIO mice.

Next, we examined how low-dose IL-2 (1,000 IU/day) improves insulin sensitivity. Since inflammation in visceral white adipose tissue, but not in inguinal white adipose tissue, is closely associated with systemic insulin resistance [26], we conducted flow cytometry (FACS) analysis of gWAT after vehicle or low-dose IL-2 administration. We examined the changes in the polarization of CD4⁺T cells and ATMs, which are known to be associated with adipose tissue insulin sensitivity

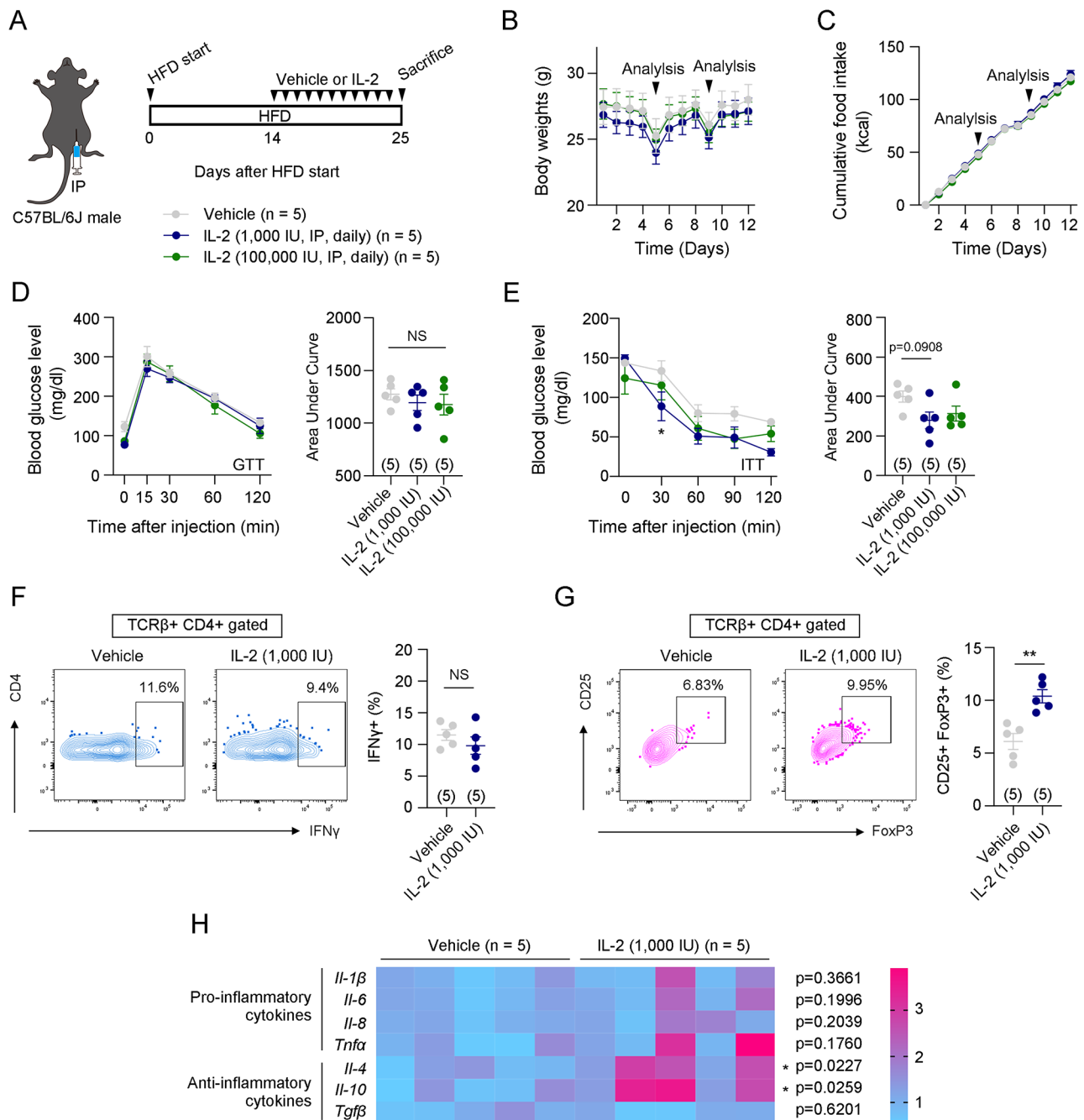


Fig. 1 Systemic IL-2 administration improved insulin sensitivity in HFD-induced obese mice. **A**. Illustration of systemic IL-2 administration and the experimental timeline. **B and C**. Changes in body weight and food intake during intraperitoneal injection of vehicle or IL-2. The arrows indicate the time points of metabolic analysis (n=5). **D and E**. Glucose and insulin tolerance tests were performed on the 5th and 9th day after the first vehicle or IL-2 administration (n=5). **F and G**. Flow cytometry analysis of Th1 cells (CD45+TCRβ+CD4+IFNγ+) and Treg cells (CD45+TCRβ+CD4+CD25+FoxP3+) in gWATs of vehicle and IL-2 [1,000 IU] groups (n=5). **H**. Comparison of mRNA expressions of inflammation-related genes, including *Il-1β*, *Il-6*, *Il-8*, *Tnfa*, *Il-4*, *Il-10*, and *Tgfb* (n=5). Results are presented as mean ± SEM. Statistical analyses were performed using one-sided two-way ANOVA (**B, C, D** [left]), one-sided one-way ANOVA (**D** [right], **E** [right]), and two-sided Student's t-test (**F, G, H**). *p < 0.05, **p < 0.01, and ***p < 0.001 between the indicated groups. NS, not significant

[27–29]. The gating strategies regarding these cells are presented in Fig. S2A and S2B. The results showed that low-dose IL-2 significantly increased the population of CD4+CD25+FoxP3+Treg cells (Fig. 1G).

However, the percentage of IFNγ+Th1 cells and the polarization of ATMs (CD11c+CD206- M1-like ATM and CD11c- CD206+M2-like ATM) were unaltered by low-dose IL-2 administration compared to those in

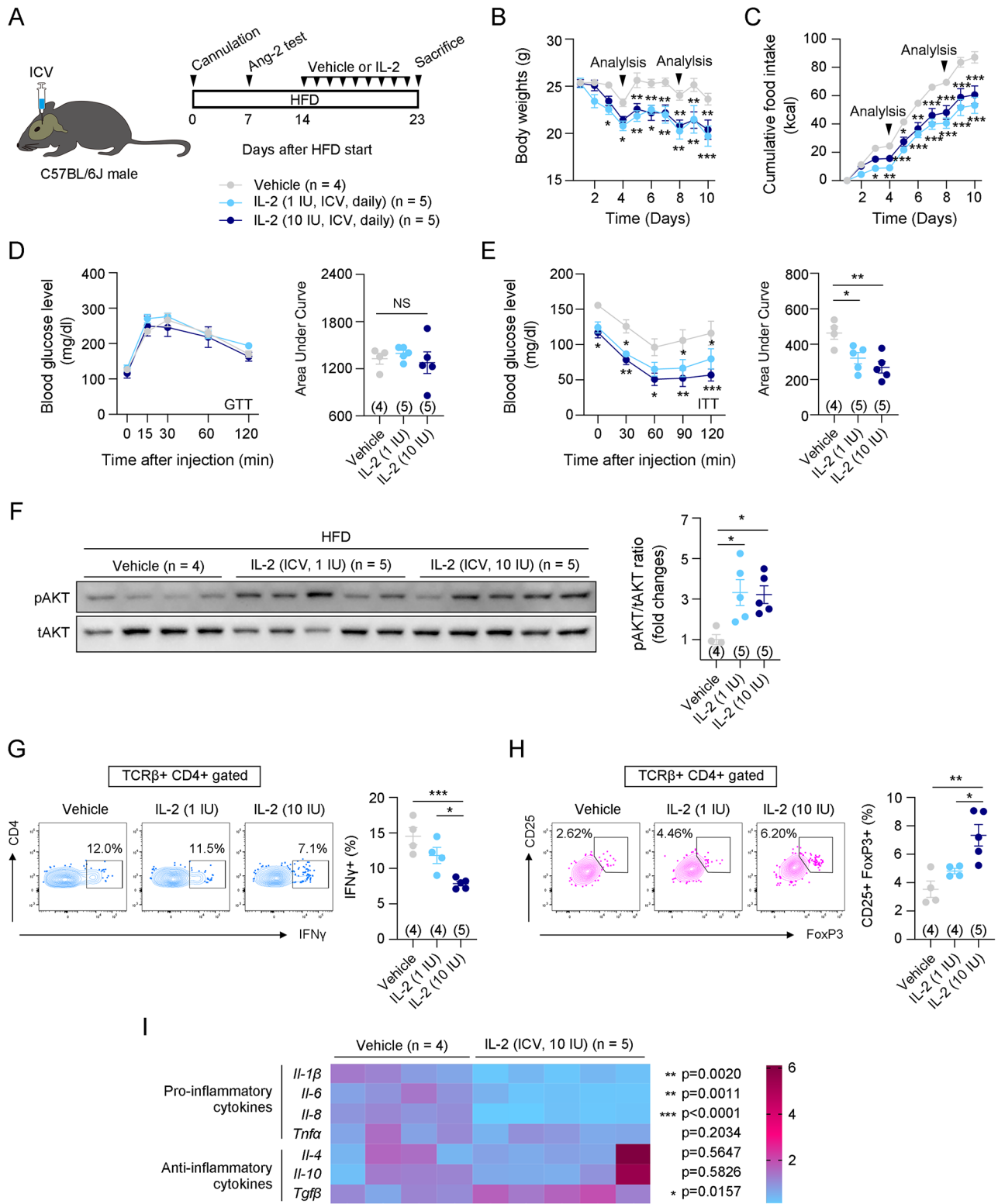


Fig. 2 (See legend on next page.)

(See figure on previous page.)

Fig. 2 Central IL-2 administration improved insulin sensitivity in HFD-induced obese mice. **A**. Illustration of central IL-2 administration and the experimental timeline. **B** and **C**. Changes in body weight and food intake during intraperitoneal injection of vehicle or IL-2. The arrows indicate the time points of metabolic analysis ($n=4$ for vehicle, $n=5$ for IL-2 [1 IU] and IL-2 [10 IU]). **D** and **E**. Glucose and insulin tolerance tests were performed on the 4th and 8th day after the first vehicle or IL-2 administration ($n=4$ for vehicle, $n=5$ for IL-2 [1 IU] and IL-2 [10 IU]). **F**. Western blot data and quantification of pAKT and tAKT after insulin administration in the vehicle, IL-2 [1 IU], and IL-2 [10 IU] groups ($n=4$ for vehicle, $n=5$ for IL-2 [1 IU] and IL-2 [10 IU]). **G** and **H**. Flow cytometry analysis of Th1 cells (CD45+TCR β +CD4+IFN γ +) and Treg cells (CD45+TCR β +CD4+CD25+FoxP3+) in gWATs of vehicle, IL-2 [1 IU], and IL-2 [10 IU] groups ($n=4$ for vehicle and IL-2 [1 IU] and $n=5$ for IL-2 [10 IU]). **I**. Comparison of mRNA expressions of inflammation-related genes, including *Il-1 β* , *Il-6*, *Il-8*, *Tnfa*, *Il-4*, *Il-10*, and *Tgfb* ($n=4$ for vehicle and $n=5$ for IL-2 [10 IU]). Results are presented as mean \pm SEM. Statistical analyses were performed using one-sided two-way ANOVA (**B**, **C**, **D** [left], **E** [left]), one-sided one-way ANOVA (**D** [right], **E** [right], **F**, **G**, **H**), and two-sided Student's t-test (**I**). * $p < 0.05$, ** $p < 0.01$, and *** $p < 0.001$ between the indicated groups. NS, not significant

the vehicle-administered group (Fig. 1F and Fig. S3). In addition, although lower doses of IL-2 (10 IU/day and 100 IU/day) did not significantly affect Th1 and Treg cell polarization in gWAT, the 100 IU IL-2 dose showed a trend toward increasing Treg cells (Fig. S4A, B). Next, we evaluated mRNA expression levels of pro-inflammatory cytokines such as *Il-1 β* , *Il-6*, *Il-8*, and *Tnfa*, as well as anti-inflammatory cytokines like *Il-4*, *Il-10*, and *Tgfb* in gWAT from mice administered 1,000 IU IL-2 daily. Anti-inflammatory cytokines *Il-4* and *Il-10* were significantly upregulated, while pro-inflammatory cytokine levels and *Tgfb* remained unchanged (Fig. 1H). These findings suggest that low-dose IL-2 exerts anti-inflammatory effects by promoting Treg cell differentiation and enhancing the expression of anti-inflammatory cytokines in gWAT.

Central IL-2 administration improved insulin sensitivity in HFD-fed obese mice.

The hypothalamus controls appetite and energy metabolism in the body [30]. Inflammation of the hypothalamus is closely associated with metabolic disorders, including insulin resistance [17]. Cumulative evidence suggests that reducing hypothalamic inflammation improves insulin sensitivity in mice with diet-induced obesity and diabetes [19, 31, 32]. We examined whether IL-2-induced increases in insulin sensitivity occurred through hypothalamic regulation. To examine this, 1 and 10 IU/day of IL-2 were centrally administered, and body weight, food intake, glucose metabolism, and insulin metabolism were examined (Fig. 2A). Notably, central administration of IL-2 dramatically improved insulin sensitivity in HFD-fed obese mice, along with weight loss and appetite suppression (Fig. 2B-E). We observed that weight loss induced by central IL-2 administration was due to reduced adipocyte size in BAT and iWAT (Fig. S5A). Central IL-2 administration significantly increased the expression of lipolysis-related genes, such as *Scad* and *Atgl* in iWAT, and *Perilipin* in BAT (Fig. S5B). Additionally, UCP-1 protein levels and mRNA expression of adrenergic receptors, including β 2-adrenergic receptor (*Adrb2*) and β 3-adrenergic receptor (*Adrb3*), indicating that IL-2 promotes sympathetic activation, lipolysis, and thermogenesis (Fig. S5C, D). However, in gWAT, central IL-2 administration did not significantly reduce adipocyte size, nor did it affect the expression of lipolysis- and

thermogenesis-related genes or adrenergic receptors (Fig. S5A, B, D). Instead, central IL-2 administration significantly enhanced insulin-induced pAKT/tAKT levels in gWAT, but not in BAT or iWAT (Fig. 2F and Fig. S6). These results suggest that central IL-2 administration has distinct effects depending on the type of adipose tissue.

Recent studies indicated that sympathetic efferent signals originating from the central nervous system contribute to the polarization of immune cells in peripheral tissues [33]. To investigate the cause of the central IL-2-induced improvement in insulin sensitivity, we conducted FACS analysis of gWAT. Notably, central IL-2 administration significantly increased CD25+FoxP3+Treg cells and decreased IFN γ +Th1 cells. However, the polarization of ATMs, as well as the percentage of B cells, T cells, myeloid cells, monocytes, neutrophils, CD4 T cells, CD8 T cells, CD4+central memory T (TCM) cells, CD8+effector memory T (TEM) cells, CD8+TCM cells, and CD8+naïve T cells, remained unchanged (Fig. 2G, H and Fig. S7A, D-I). However, a decrease in CD4+TEM cells and an increase in CD4+naïve T cells were observed, indicating that CD4+T cells may be most affected by central IL-2 administration (Fig. S7H). The related gating strategies are shown in Fig. S7B and S7C. We next assessed the mRNA expression levels of inflammatory cytokines in the gWAT of mice administered with central IL-2. This analysis revealed a significant reduction in pro-inflammatory cytokines, such as *Il-1 β* , *Il-6*, and *Il-8*, along with an increase in the anti-inflammatory cytokine *Tgfb* (Fig. 2I). These results indicate that central IL-2 administration regulates CD4+T cell differentiation and cytokine expression in gWAT through the neuro-immune axis, leading to an immunoregulatory effect and enhanced insulin sensitivity.

Previous studies have shown that reduced calorie intake is associated with improved insulin sensitivity [34, 35]. To determine whether the central IL-2-induced improvement in insulin sensitivity was due to reduced food intake, we conducted metabolic analyses comparing the central IL-2 group with a pair-fed group (Fig. 3A). The pair-fed mice were given the same amount of food consumed by the central IL-2 group over the previous 24 h. The results showed that central IL-2 administration

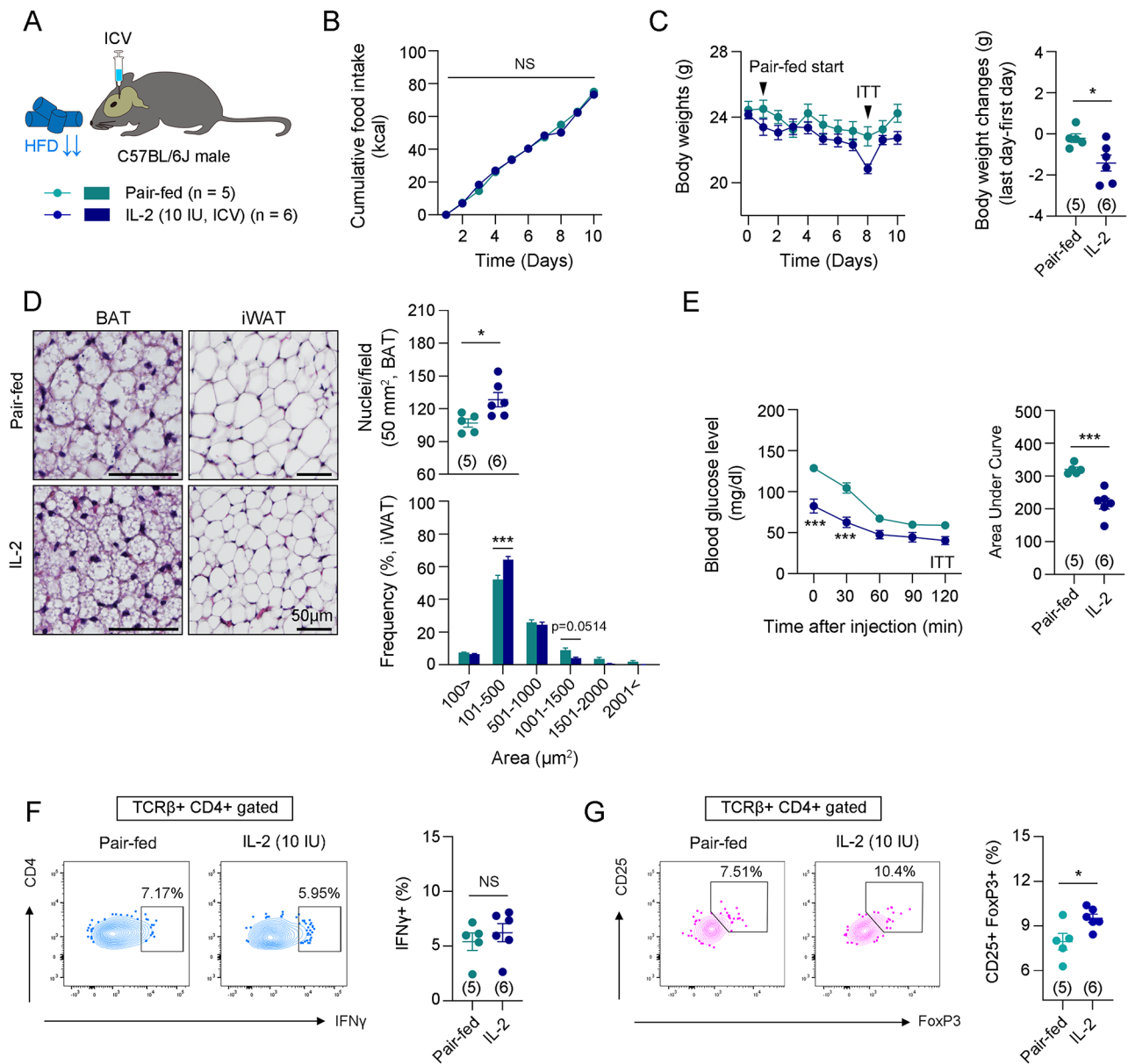


Fig. 3 Central IL-2 administration improved insulin sensitivity compared to pair-fed mice. **A**. Illustration of central IL-2 administration. **B**. Cumulative food intakes between the vehicle-administered pair-fed group and the IL-2 administered-group ($n=5$ for pair-fed group and $n=6$ for IL-2 group). **C**. Graphs of body weights and body weight changes between the vehicle-administered pair-fed group and the IL-2 administered group ($n=5$ for pair-fed group and $n=6$ for IL-2 group). **D**. Representative images and quantification of H&E staining of BAT and iWAT of the pair-fed or IL-2-administered mice ($n=5$ for pair-fed group and $n=6$ for IL-2 group). Scale bars: 50 μm. **E**. Insulin tolerance test was performed on the 8th day after starting pair-feeding ($n=5$ for pair-fed group and $n=6$ for IL-2 group). **F** and **G**. Flow cytometry analysis of Th1 cells (CD45 + TCRβ + CD4 + IFNγ+) and Treg cells (CD45 + TCRβ + CD4 + CD25 + FoxP3+) in gWATs ($n=5$ for pair-fed group and $n=6$ for IL-2 group). Results are presented as mean ± SEM. Statistical analyses were performed using one-sided two-way ANOVA (**B**, **C** [left], **D** [lower], **E** [left]) and two-sided Student's t-test (**C** [right], **D** [upper], **E** [right], **F**, **G**). * $p < 0.05$ and *** $p < 0.001$ between the indicated groups. NS, not significant

resulted in a further reduction in body weight, adipocyte size in BAT and iWAT, and improved insulin sensitivity compared to vehicle-administered pair-fed mice (Fig. 3B–E). Additionally, IL-2 administration significantly increased the percentage of CD25+FoxP3+Treg cells, but not IFN γ +Th1 cells, compared to the pair-fed mice (Fig. 3F, G). These findings suggest that the improvement in insulin sensitivity and Treg cell polarization induced by central IL-2 is mediated by neuro-immune interactions rather than its anorexigenic effects.

Central IL-2 stimulated the sympathetic nervous system by inducing hypothalamic microgliosis and POMC activation

The hypothalamus plays an important role in regulating the sympathetic nervous system (SNS) [36, 37]. When the SNS is activated, corticosterone is released into the bloodstream via the hypothalamic-pituitary-adrenal gland (HPA) axis, and NE levels are increased in peripheral tissues [38]. Because both corticosterone and NE have anti-inflammatory effects [39–41], we investigated whether central IL-2 alters immune cell polarization in gWAT through SNS activation. Central IL-2 administration significantly increased NE levels in gWAT 30 min after injection (Fig. 4A). Additionally, 3'-5'-cyclic adenosine monophosphate (cAMP) signaling, an intracellular messenger activated by sympathetic activity [42], was also increased in gWAT (Fig. 4B). This result indicated that central IL-2 administration triggered sympathetic signaling to gWAT. However, the circulating corticosterone levels did not increase following central IL-2 administration (Fig. 4C). In the hypothalamus, the activity of POMC neurons is closely associated with SNS activation [43, 44]. We observed that central IL-2 administration significantly increased the number of cFos+POMC neurons in the hypothalamus after 30 min (Fig. 4D). Remarkably, this phenomenon coincided with the increase in NE levels in the gWAT (Fig. 4A). These results indicate that central IL-2 administration can induce adrenergic signaling in gWAT by activating hypothalamic POMC neurons and the SNS.

Next, we investigated how central IL-2 activates POMC neurons. Given that previous studies have shown a negative correlation between hypothalamic microgliosis and POMC activation [19, 45], we hypothesized that central IL-2 administration would suppress HFD-induced hypothalamic microgliosis. First, we examined whether the three chains of IL-2R, such as IL-2R α , IL-2R β , and IL-2R γ , were expressed in the microglia. Immunostaining data revealed that all these receptors were expressed in hypothalamic microglia (Fig. 4E). Additionally, 80.75% \pm 2.75% of IL-2R α , 92.98% \pm 1.51% of IL-2R β , and 96.15% \pm 1.04% of IL-2R γ expressed on hypothalamic microglia, suggesting the co-expression of all three IL-2R receptors on the majority of these cells (Fig. 4E). The hypothalamic

expression of the receptors was unchanged by HFD compared to CD (Fig. S8A). Contrary to our expectations, microgliosis in the hypothalamus was more enhanced in the centrally IL-2-administered mice than in vehicle-administered DIO mice (Fig. 4F). Moreover, contrary to previous reports linking hypothalamic microgliosis closely with pro-inflammation, centrally administered IL-2 increased the expression of anti-inflammatory cytokines, such as *Il-4* and *Il-10*, highlighting the anti-inflammatory properties of IL-2 (Fig. S8B). Studies have shown that enhanced hypothalamic microgliosis activates POMC neurons by direct binding, which leads to improved systemic metabolism [20, 21]. In our study, the number of physical contacts between activated microglia and POMC neurons was increased following central IL-2 administration, while the number of hypothalamic POMC neurons was unchanged (Fig. 4F). These results suggest that the SNS activation induced by central IL-2 administration occurs via hypothalamic microgliosis and POMC activation.

Sympathetic denervation in gWAT reversed improved insulin sensitivity induced by IL-2

We investigated whether the enhanced insulin sensitivity induced by central IL-2 administration could be prevented by blocking the sympathetic neural circuit between the hypothalamus and adipose tissue. Upon central IL-2 administration, we compared body weight, food intake, insulin sensitivity, and immune cell polarization between mice injected with 6-OHDA (dissolved in 1% AA) into the gWAT to deplete the SNS and mice injected with 1% AA into the gWAT (Fig. 5A). Successful depletion of the sympathetic nerve terminals was confirmed by immunoblotting of TH (Fig. 5B). Sympathetic denervation did not affect changes in body weight, food intake, or central IL-2-induced hypothalamic microgliosis or POMC activation (Fig. 5C, D and Fig. S9A, B). However, it worsened insulin sensitivity in response to central IL-2 administration (Fig. 5E). Furthermore, a significant decrease in CD25+FoxP3+Treg cells and an increase in CD11c+CD206- M1-like ATMs were observed, while IFN γ +Th1 cells and CD11c- CD206+M2-like ATMs remained unchanged (Fig. 5F, G, and Fig. S9C). Taken together, these results indicate that IL-2-induced improved insulin sensitivity and immune cell polarization in the gWAT occurs through SNS activation.

Discussion

In the present study, we investigated whether IL-2 enhances insulin sensitivity by altering immune cell polarization and inflammatory cytokine expression in the gWAT of HFD-induced obese mice. We demonstrated that IL-2 administration via both the systemic and central routes enhanced systemic insulin sensitivity.

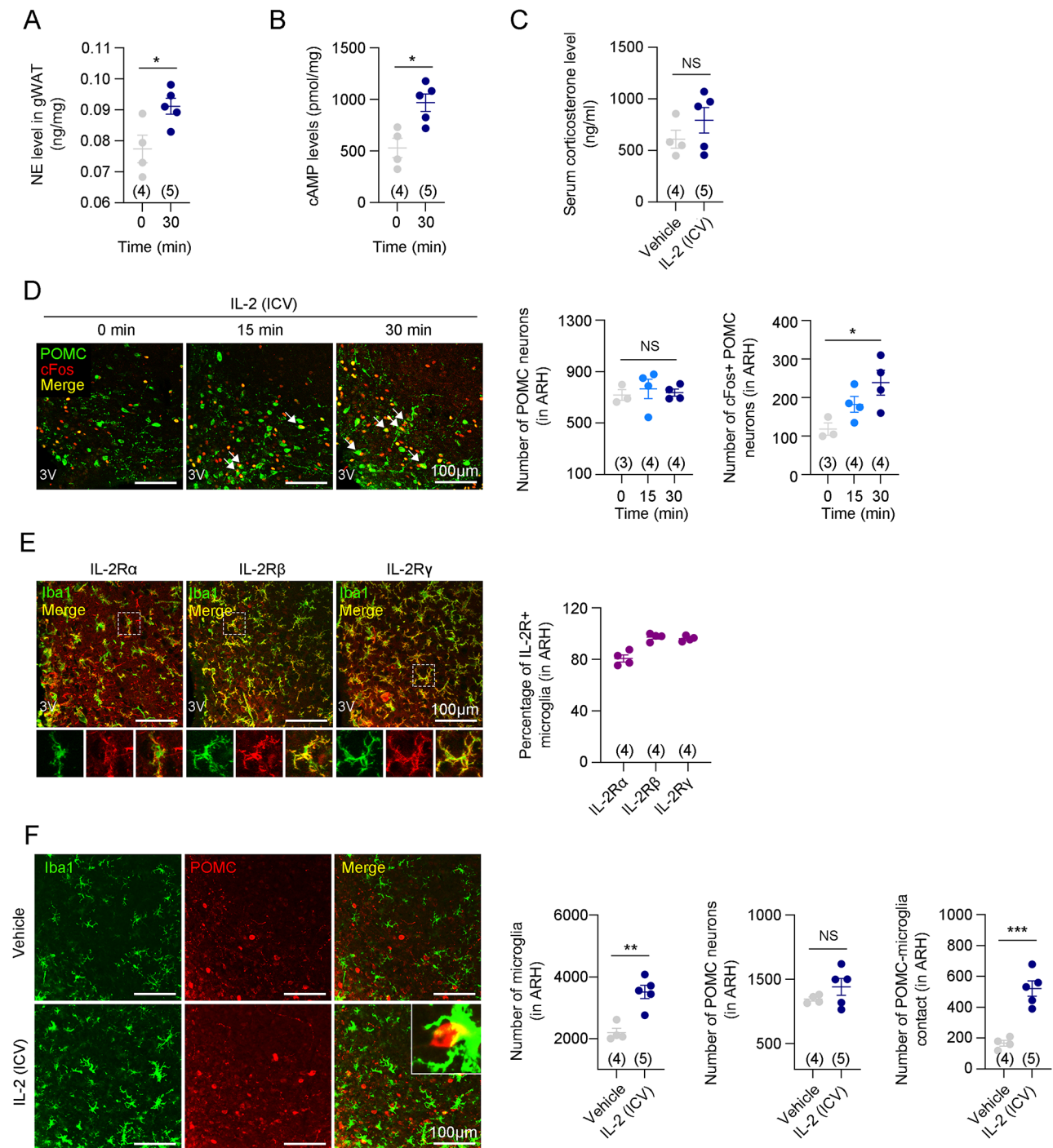


Fig. 4 Central IL-2 administration stimulated the SNS through the activation of hypothalamic microglia and POMC neurons. **A**. Time-dependent concentration of norepinephrine levels in gWAT at 0 and 30 min after central IL-2 administration ($n=4$ for 0 min and $n=5$ for 30 min). **B**. cAMP levels in gWAT 30 min after central IL-2 administration ($n=4$ for 0 min and $n=5$ for 30 min). **C**. Serum corticosterone level 30 min after central IL-2 administration ($n=4$ for the vehicle and $n=5$ for the IL-2 groups). **D**. Double immunostaining images and quantification of POMC and cFos at 0, 15, and 30 min after central administration of IL-2 in the ARH ($n=3$ for 0, and $n=4$ for 15 and 30 min). Scale bars: 100 μ m. **E**. Representative immunostaining images and quantifications of IL-2R α , IL-2R β , and IL-2R γ expressions in the hypothalamic microglia ($n=4$). Scale bars: 100 μ m. **F**. Double immunostaining images and quantification of Iba1 and POMC after central administration of vehicle or IL-2 ($n=4$ for the vehicle and $n=5$ for the IL-2 groups). Scale bars: 100 μ m. Results are presented as mean \pm SEM. Statistical analyses were performed using one-sided one-way ANOVA (**D**) and two-sided Student's t-test (**A, B, C, F**). * $p<0.05$, ** $p<0.01$, and *** $p<0.001$ between the indicated groups. NS, not significant

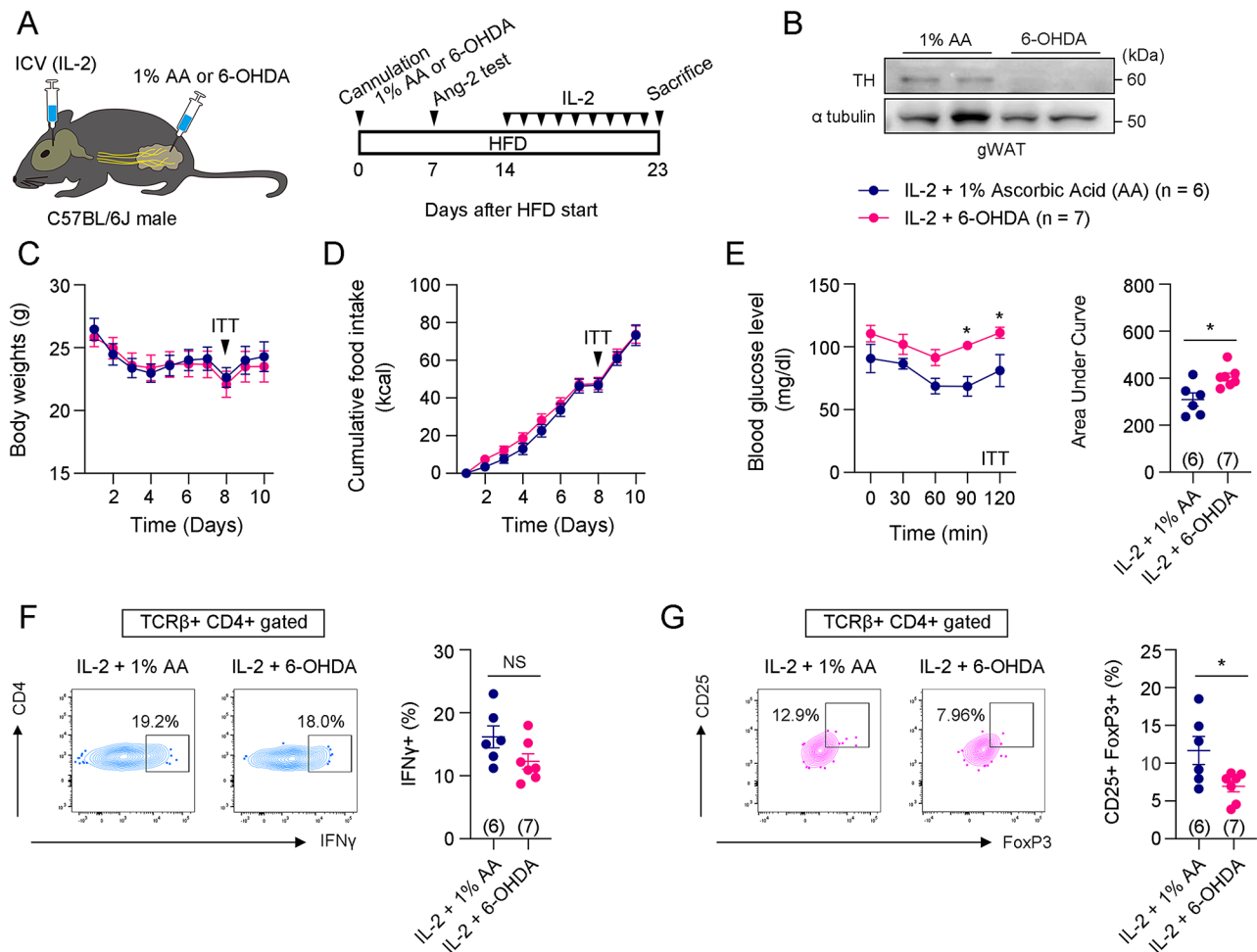


Fig. 5 Sympathetic denervation reversed improved insulin sensitivity induced by central IL-2 administration. **A** Illustration and experimental timetable of central IL-2 administration and 1% ascorbic acid (AA) or 6-OHDA injection into gWAT. **B** Representative western blotting images of TH and α -tubulin in gWAT of mice injected with 1% AA or 6-OHDA into gWAT. **C and D** Changes in body weight and food intake during central IL-2 administration after 1% AA- or 6-OHDA-injected mice ($n=6$ for the 1% AA and $n=7$ for the 6-OHDA groups). **E** Insulin tolerance tests performed on the 8th day after the vehicle or IL-2 administration ($n=6$ for the 1% AA and $n=7$ for the 6-OHDA groups). **F and G** Flow cytometry analysis of Th1 cells (CD45 + TCR β + CD4 + IFN γ +) and Treg cells (CD45 + TCR β + CD4 + CD25 + FoxP3+) in gWATs ($n=6$ for the 1% AA and $n=7$ for the 6-OHDA groups). Results are presented as mean \pm SEM. Statistical analyses were performed using two-sided Student's t-test (**E** [right], **F**, **G**) and one-sided two-way ANOVA (**C**, **D**, **E** [left])

Systemic administration of low-dose IL-2 not only increased immunoregulatory CD25+FoxP3+Treg cells and anti-inflammatory cytokines in gWAT but also improved systemic insulin sensitivity in DIO mice. Additionally, central administration of IL-2 improved insulin sensitivity by lowering the polarization of Th1 cells and the expression of pro-inflammatory cytokines, and by enhancing the polarization of Treg cells and *Tgfb* expression in gWAT through SNS activation. Central IL-2-induced SNS activation was closely associated with hypothalamic microgliosis and POMC activation. Our findings indicate that IL-2 enhances insulin sensitivity by directly modulating immune cell polarization in gWAT or by activating the SNS, highlighting the significance of the “neuro-immune axis” (Fig. 6).

Low-dose IL-2 induces CD4+T cell polarization into Treg cells through binding to IL-2R $\alpha\beta\gamma$ with high affinity, while high-dose IL-2 stimulates cytotoxic T cells by binding to IL-2R $\beta\gamma$ with intermediate affinity [9]. Accordingly, high-dose IL-2 has been explored in cancer therapy, although overcoming challenging side effects such as VLS remains necessary [6, 7]. However, research on applying low-dose IL-2 to inflammatory diseases such as obesity and metabolic disorders is largely unexplored, despite the known contribution of Treg cells to improved insulin sensitivity [29]. We found that systemic administration of low-dose IL-2 improved insulin sensitivity and increased CD25+FoxP3+Treg cells in the gWAT of obese mice. These results are consistent with a previous report that the depletion of Treg cells results in insulin resistance in chow diet-fed mice [46]. Our findings suggest that

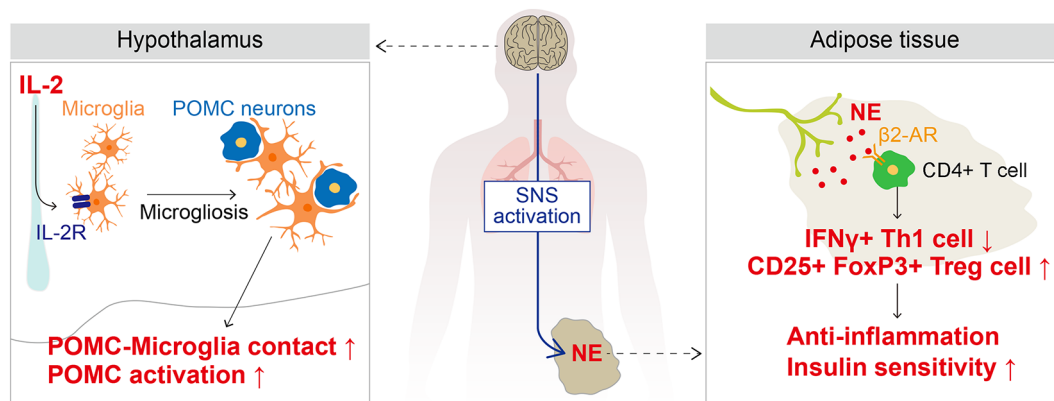


Fig. 6 Illustration of the mechanism underlying how IL-2 improves insulin sensitivity through the hypothalamic-immune axis

low-dose IL-2 administration could potentially be useful for treating inflammatory diseases such as metabolic disorders in the future.

We found that IP and central IL-2 administrations act through different mechanisms to increase Treg cells in the gWAT of DIO mice and improve insulin sensitivity. IL-2 administered IP at 1,000 IU/day directly increased Treg cell percentages in gWAT, whereas central IL-2 administration increased Treg cells via SNS activation. In fact, IP-administered IL-2 was detected only in the median eminence (ME), where the blood-brain barrier (BBB) is absent, and barely reached the arcuate nucleus (ARH), where POMC neurons are located (Fig. S10A). Additionally, systemically administered IL-2 did not result in hypothalamic microgliosis or POMC neuron activation, unlike ICV-administered IL-2, indicating that these mechanisms are distinct (Fig. S10B, C). These findings are consistent with previous studies showing that circulating IL-2 does not cross the BBB [47]. However, since the ME is part of the circumventricular organs lacking a BBB [48], the uptake of circulating factors under specific conditions cannot be entirely ruled out. Therefore, further research is needed to investigate whether circulating IL-2 can cross the BBB during inflammatory conditions.

Hypothalamic microgliosis has been recognized to induce hypothalamic inflammation by producing pro-inflammatory cytokines such as IL-1 β , IL-6, and TNF α [19, 31, 32]. Hypothalamic inflammation decreases the activity of hypothalamic POMC neurons and disrupts POMC neural circuits, ultimately resulting in metabolic disorders such as glucose intolerance and insulin resistance [17]. We observed that central IL-2 administration enhanced hypothalamic microgliosis and significantly activated POMC neurons. Although these unexpected findings contradict previous reports, some studies have suggested that hypothalamic microgliosis contributes to the activation of POMC neurons [20, 21]. Jin et al. showed that central administration of the TLR2 ligand

Pam3CSK4 induces microgliosis and activation of POMC neurons by increasing glutamatergic innervation onto POMC neurons [20]. Douglass et al. recently reported that increased NF- κ B signaling in microglia and chemogenetic activation of hypothalamic microglia enhance hypothalamic POMC activation, thereby enhancing systemic metabolism in obesity [21]. These findings highlight the need for further research on the complex relationships among hypothalamic microgliosis, POMC activation, and systemic metabolism.

It has been established that the SNS possesses anti-inflammatory properties [39, 41]. NE, released from sympathetic nerve terminals, not only stimulates neighboring T cells to promote acetylcholine secretion through the β_2 -adrenergic receptor (AR) but also increases the population of Treg cells via the β_2 -AR-protein kinase A (PKA) canonical pathway [49, 50]. The acetylcholine released by T-ChAT cells exerts anti-inflammatory effects via the α_7 -nicotinic acetylcholine receptor (α_7 nAChR) expressed in macrophages [51]. In our study, NE secretion in gWAT was increased by central IL-2 administration, which resulted in an increase in Treg cell population and a decrease in Th1 cell population. This phenomenon coincided with the timing of POMC activation induced by hypothalamic microgliosis, indicating a close association between hypothalamic POMC activation and gWAT NE secretion. Since hypothalamic POMC neurons have been known to activate the SNS [43, 44], our results underscore the potential role of hypothalamic POMC neurons in regulating immune cells in peripheral tissues.

SNS activation is closely associated with the catabolic pathways of adipose tissues, such as BAT and iWAT, subsequently reducing fat mass [44, 52]. In our previous research, we demonstrated that the activation of POMC neurons as well as central β -endorphin administration activate the SNS and contribute to the catabolic program of adipose tissues [44]. In this study, central IL-2 administration reduced adipocyte size and increased UCP-1 expression in BAT and iWAT, although no significant

reduction in adipocyte size was observed in gWAT. These findings are consistent with a recent study involving mice lacking disulfide-bond A oxidoreductase-like protein (DsbA-L), a mitochondrial-localized chaperone. In that study, no differences were observed in adipocyte size in epididymal white adipose tissue (eWAT), while reductions were seen in BAT and iWAT, and systemic insulin sensitivity was significantly improved [53]. This may be explained by the distinct gene expression patterns between these tissues, with BAT expressing higher levels of sympathetic markers like tyrosine hydroxylase (Th) and fatty acid oxidation markers like carnitine palmitoyltransferase 1 (Cpt1b) compared to gWAT [54]. In contrast, gWAT expresses higher levels of adiponectin, which regulates systemic insulin sensitivity, compared to BAT [54–56]. In our study, central IL-2 administration significantly increased the expression of adrenergic receptors *Adrb2* and *Adrb3* in BAT and iWAT, but not in gWAT (Fig. S5D). Since sympathetic activity can vary depending on conditions such as inflammatory disorders or cold exposure, further investigations into the changes in adipose tissue under various experimental or disease conditions are crucial.

The role of IL-2R in T cells is well-known compared to that in other immune cells [9, 10]. The different affinities of each of the three chains of IL-2R against IL-2 can lead to variations in T-cell differentiation, and this principle is utilized in cancer therapy and anti-inflammatory treatment research [4, 5]. In our study, we demonstrated for the first time that all three IL-2R chains are highly expressed in hypothalamic microglia, and that microglia were activated following IL-2 administration. Notably, central IL-2 administration increased the mRNA expression of IL-2R α in the hypothalamus (Fig. S8C), along with elevated levels of anti-inflammatory cytokines such as IL-4 and IL-10 (Fig. S8B). These findings indicate a similar trend where low-dose IL-2 stimulates Treg polarization through IL-2R $\alpha\beta\gamma$, unlike high-dose IL-2 binding to IL-2R $\beta\gamma$ [9]. Our data revealed that IL-2 may directly act on microglia, thereby activating them with anti-inflammatory properties. However, further investigation is required to understand the precise molecular mechanism of microglial IL-2R signaling in anti-inflammation.

Conclusions

In our study, we demonstrated that systemic or central IL-2 administration improves insulin sensitivity through T cell polarization in gWAT, emphasizing the importance of the neuro-glial interaction as well as the neuro-immune axis. Our study not only suggests the potential use of IL-2 in treating inflammatory disorders, such as metabolic disorders, but also highlights the fact that central nervous system signaling can contribute to peripheral tissue immune cell polarization and cytokine

expression through hypothalamic microgliosis and neuronal activation.

Limitations of the study

(1) We found that central IL-2 administration induced changes in immune cells in gWAT through hypothalamic microgliosis and POMC activation. This process was blocked by sympathetic denervation with 6-OHDA. However, the nervous system is distributed in various tissues, including the spleen, liver, and bone marrow, through autonomic neural circuits or the HPA axis. We could not exclude the possible contributions of immune cells originating from other tissues. (2) We found that central IL-2 administration reduced pro-inflammatory cytokine expression and increased anti-inflammatory cytokine expression in gWAT through SNS activation. Additionally, central IL-2 administration altered the subpopulation of CD4+T cells (Th1 cells, Treg cells, CD4+TEM cells, and CD4+naïve T cells), while other cell populations were unaffected. This finding suggests that SNS-induced polarization of CD4+T cells play a key role in regulating gWAT inflammation. However, further studies using cell-specific depletion or knockout models are needed to clarify the precise contribution of CD4+T cells and NE/cAMP signaling in regulating gWAT inflammation and systemic metabolism. (3) The role of IL-2R chains in T cells is well-established, with different combinations of IL-2R chains determining T-cell differentiation. While our study confirmed the expression of all three IL-2R chains in hypothalamic microglia and their role in hypothalamic anti-inflammatory properties, the interaction and regulation of these chains remain unclear. Future research will be necessary to elucidate how IL-2R chains interact and function together.

Abbreviations

6-OHDA	6-hydroxydopamine
$\alpha 7nAChR$	$\alpha 7$ -nicotinic acetylcholine receptor
AA	Ascorbic acid
ACK buffer	Ammonium-Chloride-Potassium buffer
AgRP	Agouti-related protein
AR	Adrenergic receptor
ATM	Adipose tissue macrophage
BAT	Brown adipose tissue
BBB	Blood-brain barrier
BSA	Bovine serum albumin
cAMP	3'-5'-cyclic adenosine monophosphate
CD	Chow diet
ChAT	Choline acetyltransferase
Cpt1b	Carnitine palmitoyltransferase 1b
DsbA-L	Disulfide-bond A oxidoreductase-like protein
DIO	Diet-induced obesity
ELISA	Enzyme-linked immunosorbent assay
eWAT	Epididymal white adipose tissue
FACS	Fluorescence-activated cell sorting
GAPDH	Glyceraldehyde 3-phosphate dehydrogenase
gWAT	Gonadal white adipose tissue
HFD	High-fat diet
HPA axis	Hypothalamic-Pituitary-Adrenal axis
HRP	Horseradish peroxidase

HS	Horse serum
ICV	Intracerebroventricular
IFN γ	Interferon gamma
IL-2	Interleukin-2
IMDM	Iscove's modified Dulbecco's medium
IP	Intraperitoneal
IPITT	Intraperitoneal Insulin Tolerance Test
iWAT	Inguinal white adipose tissue
IU	International Unit
ME	Median eminence
NE	Norepinephrine
NF- κ B	Nuclear factor kappa B
NK cell	Natural killer cell
NOD	Nonobese diabetic
OGTT	Oral Glucose Tolerance Test
Pam3CSK4	Pam3Cys-Ser-(Lys)4
PBS	Phosphate-buffered saline
PBST	PBS containing Triton X-100
PFA	Paraformaldehyde
PKA	Protein kinase A
POMC	Pro-opiomelanocortin
RBCs	Red blood cells
RIPA buffer	Radio-immunoprecipitation assay buffer
RT	Room temperature
SNS	Sympathetic nervous system
TBST buffer	Tris-buffered saline buffer with Tween 20 detergent buffer
TCM	Central memory T cell
TCR β	T cell receptor beta
TEM	Effector memory T cell
Tg β	Transforming growth factor beta
TH	Tyrosine hydroxylase
Th1	Type 1 T helper cell
TLR2	Toll-like receptor 2
Tnfa	Tumor necrosis factor-alpha
Treg	Regulatory T cell
UCP-1	Uncoupling protein-1
VLS	Vascular leak syndrome

Supplementary Information

The online version contains supplementary material available at <https://doi.org/10.1186/s12974-024-03244-y>.

Supplementary Material 1
 Supplementary Material 2
 Supplementary Material 3
 Supplementary Material 4
 Supplementary Material 5
 Supplementary Material 6
 Supplementary Material 7
 Supplementary Material 8
 Supplementary Material 9
 Supplementary Material 10
 Supplementary Material 11
 Supplementary Material 12

Acknowledgements

We would like to thank Editage (www.editage.co.kr) for the English language editing. We used ChatGPT-3.5 to check the grammar of some sentences.

Author contributions

S. M., Y. P., and C. H. L. designed the study. S. M., Y. P., S. J., S. K., D.-G. S., and D.-C. S. performed the experiments and analyzed the data. S. M. and C. H. L.

wrote the manuscript. All authors have read and edited the manuscript and approved its final version.

Funding

This work was supported by National Research Foundation of Korea (NRF) grants (2022R1C1C1004187 and RS-2023-00223501; Bio & Medical Technology Development Program) funded by the Korean government (MSIT).

Data availability

No datasets were generated or analysed during the current study.

Declarations

Ethics approval and consent to participate

All experimental procedures were approved by the Institutional Animal Care and Use Committee (IACUC) of Hallym University (Hallym R1 #2022-72).

Consent for publication

Not applicable.

Competing interests

The authors declare no competing interests.

Received: 8 July 2024 / Accepted: 24 September 2024

Published online: 04 October 2024

References

- Morgan DA, Ruscetti FW, Gallo R. Selective in vitro growth of T lymphocytes from normal human bone marrows. *Science*. 1976;193:1007–8. <https://doi.org/10.1126/science.181845>.
- Rosenberg SA, Yang JC, Topalian SL, Schwartzentruber DJ, Weber JS, Parkinson DR, et al. Treatment of 283 consecutive patients with metastatic melanoma or renal cell cancer using high-dose bolus interleukin 2. *JAMA*. 1994;271:907–13. <https://doi.org/10.1001/jama.1994.03510360033032>.
- Rosenberg SA, Lotze MT, Muul LM, Leitman S, Chang AE, Ettinghausen SE, et al. Observations on the systemic administration of autologous lymphokine-activated killer cells and recombinant interleukin-2 to patients with metastatic cancer. *N Engl J Med*. 1985;313:1485–92. <https://doi.org/10.1056/NEJM198512053132327>.
- Fyfe G, Fisher RI, Rosenberg SA, Sznol M, Parkinson DR, Louie AC. Results of treatment of 255 patients with metastatic renal cell carcinoma who received high-dose recombinant interleukin-2 therapy. *J Clin Oncol*. 1995;13:688–96. <https://doi.org/10.1200/JCO.1995.13.3.688>.
- Rosenberg SA. IL-2: the first effective immunotherapy for human cancer. *J Immunol*. 2014;192:5451–8. <https://doi.org/10.4049/jimmunol.1490019>.
- Baluna R, Vitetta ES. Vascular leak syndrome: a side effect of immunotherapy. *Immunopharmacology*. 1997;37:117–32. [https://doi.org/10.1016/s0162-3109\(97\)00041-6](https://doi.org/10.1016/s0162-3109(97)00041-6).
- Park S, Lee S, Kim D, Kim H, Kwon YG. CU06-1004 as a promising strategy to improve anti-cancer drug efficacy by preventing vascular leaky syndrome. *Front Pharmacol*. 2023;14:1242970. <https://doi.org/10.3389/fphar.2023.1242970>.
- Skrombolas D, Frelinger JG. Challenges and developing solutions for increasing the benefits of IL-2 treatment in tumor therapy. *Expert Rev Clin Immunol*. 2014;10:207–17. <https://doi.org/10.1586/1744666X.2014.875856>.
- Raker VK, Becker C, Landfester K, Steinbrink K. Targeted activation of T cells with IL-2-coupled nanoparticles. *Cells*. 2020;9. <https://doi.org/10.3390/cells9092063>.
- Hernandez R, Pöder J, LaPorte KM, Malek TR. Engineering IL-2 for immunotherapy of autoimmunity and cancer. *Nat Rev Immunol*. 2022;22:614–28. <https://doi.org/10.1038/s41577-022-00680-w>.
- Rabinovitch A, Suarez-Pinzon WL, Shapiro AM, Rajotte RV, Power R. Combination therapy with sirolimus and interleukin-2 prevents spontaneous and recurrent autoimmune diabetes in NOD mice. *Diabetes*. 2002;51:638–45. <https://doi.org/10.2337/diabetes.51.3.638>.
- Grinberg-Bleyer Y, Baeyens A, You S, Elhage R, Fourcade G, Gregoire S, et al. IL-2 reverses established type 1 diabetes in NOD mice by a local effect on pancreatic regulatory T cells. *J Exp Med*. 2010;207:1871–8. <https://doi.org/10.1084/jem.20100209>.

13. Pérol L, Lindner JM, Caudana P, Nunez NG, Baeyens A, Valle A, et al. Loss of immune tolerance to IL-2 in type 1 diabetes. *Nat Commun*. 2016;7:13027. <https://doi.org/10.1038/ncomms13027>.
14. Dong S, Hiam-Galvez KJ, Mowery CT, Herold KC, Gitelman SE, Esensten JH, et al. The effect of low-dose IL-2 and Treg adoptive cell therapy in patients with type 1 diabetes. *JCI Insight*. 2021;6. <https://doi.org/10.1172/jci.insight.147474>.
15. Timper K, Brüning JC. Hypothalamic circuits regulating appetite and energy homeostasis: pathways to obesity. *Dis Model Mech*. 2017;10:679–89. <https://doi.org/10.1242/dmm.026609>.
16. Lee CH, Kim HJ, Lee YS, Kang GM, Lim HS, Lee SH, et al. Hypothalamic macrophage inducible nitric oxide synthase mediates obesity-associated hypothalamic inflammation. *Cell Rep*. 2018;25:934–e9465. <https://doi.org/10.1016/j.celrep.2018.09.070>.
17. Lee CH, Suk K, Yu R, Kim MS. Cellular contributors to hypothalamic inflammation in obesity. *Mol Cells*. 2020;43:431–7. <https://doi.org/10.14348/molcells.2020.0055>.
18. Thaler JP, Yi CX, Schur EA, Guyenet SJ, Hwang BH, Dietrich MO, et al. Obesity is associated with hypothalamic injury in rodents and humans. *J Clin Invest*. 2012;122:153–62. <https://doi.org/10.1172/JCI59660>.
19. Suh SB, Lee N, Kim J, Kim S, Jang S, Park JK, et al. Metformin ameliorates olanzapine-induced obesity and glucose intolerance by regulating hypothalamic inflammation and microglial activation in female mice. *Front Pharmacol*. 2022;13:906717. <https://doi.org/10.3389/fphar.2022.906717>.
20. Jin S, Kim JG, Park JW, Koch M, Horvath TL, Lee BJ. Hypothalamic TLR2 triggers sickness behavior via a microglia-neuronal axis. *Sci Rep*. 2016;6:29424. <https://doi.org/10.1038/srep29424>.
21. Douglass JD, Ness KM, Valdearcos M, Wyse-Jackson A, Dorfman MD, Frey JM, et al. Obesity-associated microglial inflammatory activation paradoxically improves glucose tolerance. *Cell Metab*. 2023;35:1613–e16298. <https://doi.org/10.1016/j.cmet.2023.07.008>.
22. Westwood JA, Darcy PK, Guru PM, Sharkey J, Pegram HJ, Amos SM, et al. Three agonist antibodies in combination with high-dose IL-2 eradicate orthotopic kidney cancer in mice. *J Transl Med*. 2010;8:42. <https://doi.org/10.1186/1479-5876-8-42>.
23. Sun Q, van de Lisdonk D, Ferrer M, Gegenhuber B, Wu M, Park Y, et al. Area Postrema neurons mediate interleukin-6 function in cancer cachexia. *Nat Commun*. 2024;15:4682. <https://doi.org/10.1038/s41467-024-48971-1>.
24. Duan Y, Zeng L, Zheng C, Song B, Li F, Kong X, et al. Inflammatory links between high fat diets and diseases. *Front Immunol*. 2018;9:2649. <https://doi.org/10.3389/fimmu.2018.02649>.
25. Zloza A, Dharmadhikari ND, Huelsmann EJ, Broucek JR, Hughes T, Kohlhapp FJ, et al. Low-dose interleukin-2 impairs host anti-tumor immunity and inhibits therapeutic responses in a mouse model of melanoma. *Cancer Immunol Immunother*. 2017;66:9–16. <https://doi.org/10.1007/s00262-016-1916-4>.
26. Macdougall CE, Wood EG, Loschko J, Scagliotti V, Cassidy FC, Robinson ME, et al. Visceral adipose tissue immune homeostasis is regulated by the crosstalk between adipocytes and dendritic cell subsets. *Cell Metab*. 2018;27:588–e6014. <https://doi.org/10.1016/j.cmet.2018.02.007>.
27. Weisberg SP, McCann D, Desai M, Rosenbaum M, Leibel RL, Ferrante AW Jr. Obesity is associated with macrophage accumulation in adipose tissue. *J Clin Invest*. 2003;112:1796–808. <https://doi.org/10.1172/JCI19246>.
28. Shimobayashi M, Albert V, Woelnerhanssen B, Frei IC, Weissenberger D, Meyer-Gerspach AC, et al. Insulin resistance causes inflammation in adipose tissue. *J Clin Invest*. 2018;128:1538–50. <https://doi.org/10.1172/JCI96139>.
29. Zeng Q, Sun X, Xiao L, Xie Z, Bettini M, Deng T. A unique population: adipose-resident regulatory T cells. *Front Immunol*. 2018;9:2075. <https://doi.org/10.3389/fimmu.2018.02075>.
30. Blouet C, Schwartz GJ. Hypothalamic nutrient sensing in the control of energy homeostasis. *Behav Brain Res*. 2010;209:1–12. <https://doi.org/10.1016/j.bbr.2009.12.024>.
31. Valdearcos M, Robblee MM, Benjamin DJ, Nomura DK, Xu AW, Koliwad SK. Microglia dictate the impact of saturated fat consumption on hypothalamic inflammation and neuronal function. *Cell Rep*. 2014;9:2124–38. <https://doi.org/10.1016/j.celrep.2014.11.018>.
32. Valdearcos M, Douglass JD, Robblee MM, Dorfman MD, Stiffler DR, Bennett ML, et al. Microglial inflammatory signaling orchestrates the hypothalamic immune response to dietary excess and mediates obesity susceptibility. *Cell Metab*. 2017;26:185–e1973. <https://doi.org/10.1016/j.cmet.2017.05.015>.
33. Dantzer R. Neuroimmune interactions: from the brain to the immune system and vice versa. *Physiol Rev*. 2018;98:477–504. <https://doi.org/10.1152/physrev.00039.2016>.
34. Johnson ML, Distelmaier K, Lanza IR, Irving BA, Robinson MM, Konopka AR, et al. Mechanism by which caloric restriction improves insulin sensitivity in sedentary obese adults. *Diabetes*. 2016;65:74–84. <https://doi.org/10.2337/db15-0675>.
35. Yu D, Tomasiewicz JL, Yang SE, Miller BR, Wakai MH, Sherman DS, et al. Calorie-restriction-induced insulin sensitivity is mediated by adipose mTORC2 and not required for lifespan extension. *Cell Rep*. 2019;29:236–e248233. <https://doi.org/10.1016/j.celrep.2019.08.084>.
36. Kyrou I, Tsigos C. Stress hormones: physiological stress and regulation of metabolism. *Curr Opin Pharmacol*. 2009;9:787–93. <https://doi.org/10.1016/j.coph.2009.08.007>.
37. Andrews J, Ali N, Pruessner JC. Reflections on the interaction of psychogenic stress systems in humans: the stress coherence/compensation model. *Psychoneuroendocrinology*. 2013;38:947–61. <https://doi.org/10.1016/j.psyneuen.2013.02.010>.
38. Mishra G, Townsend KL. The metabolic and functional roles of sensory nerves in adipose tissues. *Nat Metab*. 2023;5:1461–74. <https://doi.org/10.1038/s42255-023-00868-x>.
39. Pongratz G, Straub RH. The sympathetic nervous response in inflammation. *Arthritis Res Ther*. 2014;16:504. <https://doi.org/10.1186/s13075-014-0504-2>.
40. Araujo LP, Maricato JT, Guereschi MG, Takenaka MC, Nascimento VM, de Melo FM, et al. The sympathetic nervous system mitigates CNS autoimmunity via β 2-adrenergic receptor signaling in immune cells. *Cell Rep*. 2019;28:3120–e31305. <https://doi.org/10.1016/j.celrep.2019.08.042>.
41. Liu K, Yang L, Wang G, Liu J, Zhao X, Wang Y, et al. Metabolic stress drives sympathetic neuropathy within the liver. *Cell Metab*. 2021;33:666–e6754. <https://doi.org/10.1016/j.cmet.2021.01.012>.
42. Bartness TJ, Liu Y, Shrestha YB, Ryu V. Neural innervation of white adipose tissue and the control of lipolysis. *Front Neuroendocrinol*. 2014;35:473–93. <https://doi.org/10.1016/j.yfrme.2014.04.001>.
43. Bell BB, Harlan SM, Morgan DA, Guo DF, Cui H, Rahmouni K. Differential contribution of POMC and AgRP neurons to the regulation of regional autonomic nerve activity by leptin. *Mol Metab*. 2018;8:1–12. <https://doi.org/10.1016/j.molmet.2017.12.006>.
44. Kang GM, Min SH, Lee CH, Kim JY, Lim HS, Choi MJ, et al. Mitohormesis in hypothalamic POMC neurons mediates regular exercise-induced high-turnover metabolism. *Cell Metab*. 2021;33:334–e3496. <https://doi.org/10.1016/j.cmet.2021.01.003>.
45. Kim J, Lee N, Suh SB, Jang S, Kim S, Kim DG, et al. Metformin ameliorates olanzapine-induced disturbances in POMC neuron number, axonal projection, and hypothalamic leptin resistance. *BMB Rep*. 2022;55:293–8. <https://doi.org/10.5483/BMBRep.2022.55.6.026>.
46. Feuerer M, Herrero L, Cipolletta D, Naaz A, Wong J, Nayer A, et al. Lean, but not obese, fat is enriched for a unique population of regulatory T cells that affect metabolic parameters. *Nat Med*. 2009;15:930–9. <https://doi.org/10.1038/nm.2002>.
47. Waguespack PJ, Banks WA, Kastin AJ. Interleukin-2 does not cross the blood-brain barrier by a saturable transport system. *Brain Res Bull*. 1994;34:103–9. [https://doi.org/10.1016/0361-9230\(94\)90005-1](https://doi.org/10.1016/0361-9230(94)90005-1).
48. Rodríguez EM, Blázquez JL, Guerra M. The design of barriers in the hypothalamus allows the median eminence and the arcuate nucleus to enjoy private milieus: the former opens to the portal blood and the latter to the cerebrospinal fluid. *Peptides*. 2010;31:757–76.
49. Rosas-Ballina M, Olofsson PS, Ochani M, Valdés-Ferrer SJ, Levine YA, Reardon C, et al. Acetylcholine-synthesizing T cells relay neural signals in a vagus nerve circuit. *Science*. 2011;334:98–101. <https://doi.org/10.1126/science.1209985>.
50. Bellinger DL, Lorton D. Sympathetic nerve hyperactivity in the spleen: causal for nonpathogenic-driven chronic immune-mediated inflammatory diseases (IMIDs)? *Int J Mol Sci*. 2018;19. <https://doi.org/10.3390/ijms19041188>.
51. Wang H, Yu M, Ochani M, Amella CA, Tanovic M, Susarla S, et al. Nicotinic acetylcholine receptor α 7 subunit is an essential regulator of inflammation. *Nature*. 2003;421:384–8. <https://doi.org/10.1038/nature01339>.
52. Caron A, Lee S, Elmquist JK, Gautron L. Leptin and brain-adipose crosstalks. *Nat Rev Neurosci*. 2018;19:153–65. <https://doi.org/10.1038/nrn.2018.7>.
53. Zhou H, Peng X, Hu J, Wang L, Luo H, Zhang J, et al. DsbA-L deficiency in T cells promotes diet-induced thermogenesis through suppressing IFN- γ production. *Nat Commun*. 2021;12:326. <https://doi.org/10.1038/s41467-020-20665-4>.
54. Zhu Q, Glazier BJ, Hinkel BC, Cao J, Liu L, Liang C, et al. Neuroendocrine regulation of Energy Metabolism Involving different types of adipose tissues. *Int J Mol Sci*. 2019;20:2707. <https://doi.org/10.3390/ijms20112707>.

55. Yamauchi T, Kamon J, Waki H, Terauchi Y, Kubota N, Hara K, et al. The fat-derived hormone adiponectin reverses insulin resistance associated with both lipodystrophy and obesity. *Nat Med.* 2001;7:941–. <https://doi.org/10.1038/90984>.
56. Maeda N, Shimomura I, Kishida K, Nishizawa H, Matsuda M, Nagaretani H, et al. Diet-induced insulin resistance in mice lacking adiponectin/ACRP30. *Nat Med.* 2002;8:731–7. <https://doi.org/10.1038/nm724>.

Publisher's note

Springer Nature remains neutral with regard to jurisdictional claims in published maps and institutional affiliations.